Microporous and Mesoporous Materials 200 (2014) 110–116

Contents lists available at ScienceDirect

Microporous and Mesoporous Materials

journal homepage: www.elsevier.com/locate/micromeso

Nature of the active sites in Al-MCM-41 nano-structured catalysts for the selective rearrangement of cyclohexanone oxime toward ε-caprolactam

Eliana G. Vaschetto [a], Gina A. Pecchi [b], Sandra G. Casuscelli [a], Griselda A. Eimer [a,*]

[a] Centro de Investigación y Tecnología Química (CITeQ) (UTN-CONICET), Facultad Regional Córdoba, Maestro López y Cruz Roja Argentina, Ciudad Universitaria, CP: 5016 Córdoba, Argentina
[b] Facultad de Ciencias Químicas, Universidad de Concepción, Casilla160-C, Concepción, Chile

ARTICLE INFO

Article history:
Received 10 June 2014
Received in revised form 25 July 2014
Accepted 15 August 2014
Available online 23 August 2014

Keywords:
Al contents
Al-MCM-41
Silanol nests
Acidic strength
ε-Caprolactam

ABSTRACT

Al-MCM-41 type nano-structured catalysts with different Al contents were prepared by direct hydrothermal synthesis. All the materials were characterized by XRD, N_2 adsorption, TEM, SEM, ICP-OES, FT-IR and adsorption of pyridine coupled to FT-IR spectroscopy. The relationship between the Al contents in the synthesis gel and final solid, the degree of Al introduction in tetrahedral coordination into the framework, the formation of nest silanols and the relative density of the acidic hydroxyl sites has been exhaustively analyzed. We could corroborate that hydroxyl groups present in silanol nests are the direct responsible of the weakly acid character of our materials. Moreover, a critical concentration of framework Al seems to be necessary to generate such nests, after which the acid sites density is strongly increased, according the framework Al amount increasing. The enhancement in the density of acidic nest silanols (active sites for the selective rearrangement of cyclohexanone oxime toward ε-caprolactam) reached by increasing the Al content, permitted to us achieve a cyclohexanone oxime conversion about 66%. The ε-caprolactam selectivity was 100% for all the evaluated catalysts, indicating that the acidic strength was kept sufficiently weak to not catalyze the formation of by-products.

1. Introduction

The investigation about porous materials is an area of intense scientific and technological activity. M41S is the collective name for a family of crystalline mesoporous molecular sieves with a regular and well defined mesopore system. MCM-41 is the member of this family [1,2] which possess a hexagonal array of unidimensional, hexagonally shaped pores in the range from 2 to 10 nm, besides a highly specific surface of up to 1000 m^2g^{-1}, a specific pore volume of up to 1.3 mL/g and a high thermal stability. In comparison with crystalline microporous zeolites, such mesoporous materials break through the pore size limit and provide the opportunity to process bulky molecules larger than 1.2 nm in diameter. Nevertheless, because of the absence of active sites of the pure siliceous MCM-41, the incorporation of heteroatoms on the silicate framework is necessary to make these materials potential catalysts. Thus, the introduction of aluminum in the mesostructure is vital from the point of view of the acid catalysis [3–7]. Moreover, it is known that these materials possesses comparatively many more Si–OH groups than microporous aluminosilicate and silicate zeolites, and such hydroxyl groups are similar to defect sites on microporous zeolites [8–11]. In this sense, Sato et al. [12] have investigated the acidity of different silanol species in zeolites reporting a higher acid character for those OH groups present on silanol nests. Recently we have claimed that such silanol nests present in our MCM-41 catalysts are generated at framework defect sites as result of the incorporation of Al inside the mesoporous framework [13]. In concordance with Sato we think that these nest silanols can act as active sites in certain reactions that require a considerably weak acidity. Thus, such sites could give a proton to a basic molecule easier than other silanols because the deprotonation species of nest silanols might be stabilized with the help of hydrogen bondings. Therefore, the structure of nest silanols in nano-structured silica can play a very important role in heterogeneous catalysis and it is in the design and synthesis of such heterogeneous catalysts where the nanotechnology can offer the most significant benefits. Nowadays, nanotechnology has opened the possibility to exquisitely control the formation of an active site and its chemical environment, that is to say control the catalyst structure and therefore its chemical properties at the atomic scale [9].

* Corresponding author. Tel./fax: +54 0351 4690585.
E-mail addresses: geimer@scdt.frc.utn.edu.ar, griseeimer@yahoo.com.ar (G.A. Eimer).

http://dx.doi.org/10.1016/j.micromeso.2014.08.030
1387-1811/

Previously, we have reported the application of the sol–gel method to synthesize Al-MCM-41 nanostructured materials from a supramolecular self-assembly process in presence of ionic surfactants as template, where certain structural and acid properties have could be tailed by controlling different synthesis parameters [6,7,13]. Moreover, considering their considerably weak acidity, these materials have been evaluated in the Beckmann rearrangement reaction of the cyclohexanone oxime (CHO) to ε-caprolactam (ε-C) [13]. ε-C is an important precursor for nylon-6 and plastics. The conventional method of preparation of ε-C from CHO via Beckmann rearrangement, using concentrated sulfuric acid as catalyst results in the formation of a large amount of by-products, especially ammonium sulfate [14]. Further problems encountered include handling of a large amount of acid and corrosion of the apparatus. To overcome these problems, many research groups come working to carry out vapor phase Beckmann rearrangement using solid catalysts [15–18]. Among the solid catalysts investigated, the Al-MCM-41 materials appear as the most interesting. Likewise, considerable attention has been focused on the type of acid sites catalytically active to promote the selective formation of ε-C. Thus, different active site types have been proposed and opposing views can be found in the literature, so that the research in this field continues to be intense [19–37]. Agreeing with some authors, we have recently suggested that weakly acid sites such as Si–OH groups present in silanol-nests, are the responsible for selectively catalyze the Beckmann rearrangement of the CHO toward ε-caprolactam [13,38–42], while strong acid sites accelerate the formation of by-products [43]. In this paper, we deepen the study about the formation of such silanol nests in the mesoporous structure as direct cause of the weakly acid character observed for our samples. Thus, the relationship between the Al content in the synthesis gel and final solid, the degree of Al introduction in tetrahedral coordination into the framework, the formation of nest silanols and the relative density of the acidic hydroxyl sites has been exhaustively analyzed. In addition, the Beckmann rearrangement reaction of CHO was performed on the catalysts synthesized with different Al contents in order to analyze the influence of the amount and nature of the generated active sites over the yield and selectivity to ε-C.

2. Experimental

2.1. Synthesis

The Al-MCM-41 mesoporous materials with different Al content have been prepared as follows: cetyltrimethylammonium bromide (CTMABr, Merck, 99%) was dissolved in H_2O–NaOH solution and after heating (308–313 K) to dissolve the surfactant, the tetraethylorthosilicate (TEOS, Aldrich, 98%) was added and stirred for 30 min. After the sodium aluminate (Johnson Matthey) addition, the synthesis gel (molar composition: Si/Al = 10, 20, 30, 40, 60, 80 and 100, NaOH/Si = 0.50, CTMABr/Si = 0.12, H_2O/Si = 132 and pH = 11.25), was stirred at room temperature for 7 h and hydrothermal treated at 373 K for 6 days. The final solid was filtered, washed with distilled water and dried at 333 K overnight. To remove the template, the samples were heated under N_2 flow up to 773 K and kept at this temperature for 6 h; they were then calcined at 773 K under air flow for 6 h. The calcined samples were named as Al-M(x), where "x" is the Si/Al initial molar ratio.

2.2. Characterization

The X-ray diffraction (XRD) patterns were recorded in air at room temperature on a Philips PW 3830 diffractometer with Cu Kα radiation (λ = 1.5418 Å) in the range of 2θ from 1.5 to 7. The specific surface area, the pore size distribution and the total pore volume were determined from N_2 adsorption–desorption isotherms obtained at 77 K using a Micromeritics TriStar II 3020 V1.03 (V1.03). The surface area was determined by the Brunauer–Emmett–Teller (BET) method in the pressure range of P/P_0: 0.01–0.25. The pore size distributions were determined by the Barrett–Joyner–Halenda (BJH) method, based on the Kelvin equation. The scanning electron microscopy (SEM) images of the materials were obtained in a JEOL JSM-6380 LV. Gold coverage was applied to make samples conductive. The acceleration voltage was 20 kV. Moreover, the solids were analyzed by Transmission Electron Microscopy (TEM) with a JOEL JEM-1200 EX II, working voltage: 120 kV. A small drop of the dispersion (sample in solution water–ethanol 50%) was deposited on copper grid and then evaporated in air at room temperature. The Al and Na contents was determined by inductively coupled plasma optical emission spectroscopy (ICP-OES), using a VISTA-MPC CCD simultaneous ICP-OES-VARIAN. Infrared analysis of the samples was recorded on a JASCO 5300 FT-IR spectrometer in the range 400–1600 cm^{-1}, named the fingerprint zone of the material, for the KBr-pelletized samples. To examine the presence of silanol groups on the samples the hydroxyl zone of the FT-IR spectra has been analyzed. For this, self-supported wafers of the samples were prepared, placed in a thermostatized connected to a vacuum line and evacuated for 7 h at 673 K under a dynamic vacuum; residual pressure was smaller than 10^{-3} Pa. After cooling to room temperature, the FT-IR spectrum of each sample was recorded (background spectrum). In addition, in order to evaluate the strength and type of acid sites, FT-IR spectral measurements of pyridine adsorbed on the samples were performed. Thus, after the background spectrum was obtained, the solid wafer was exposed to pyridine vapors until saturate the system to 46 mm Hg at room temperature. Then, the spectrum was recorded after the pyridine excess desorption by evacuation for 1 h.

2.3. Catalytic reactions

The freshly calcined catalysts were used for reactions which were carried out in a down flow fixed bed tubular glass reactor (i.d.= 8 mm and 35 cm length) at atmospheric pressure using 0.2 g of the catalyst. The reactor was placed inside a temperature controlled vertical furnace (593 K). A solution of 10 wt.% CHO in 1-hexanol was fed using a syringe pump (5.6 mL/min). CHO employed was 97% pure (Fluka). The contact time (W/F = 40 gh/mol) refers to the weight of catalyst (g) over the feed rate of CHO (mol/h). Nitrogen was used as the carrier gas (30 cm^3/min). The reaction products were collected in a receiver after cooling with ice cold water. The samples were analyzed using a Perkin Elmer gas chromatograph (Clarus 500) with a capillary column (ZB-1, 30 m × 0.53 mm i.d.) and a flame ionization detector (FID). The product identification was done by GC–MS (PerkinElmer - Clarus 560S) with a capillary column (E-5 30 m × 0.53 mm i.d.). Moreover, the reaction products were also analyzed by comparison with chromatographic standards. The conversion was expressed in moles%.

3. Results and discussion

3.1. Structural characterization

Table 1 shows the physicochemical, textural and structural properties and chemical composition of the catalysts synthesized in this work.

Fig. 1 shows the XRD patterns obtained for all of the materials. The well-resolved diffraction lines observed for all samples in the

Table 1
Physico-chemical properties and infrared data for the calcined solids.

Sample	Si/Al[a]	a_0[b] (nm)	Area ($m^2\ g^{-1}$)	Al content (wt.%)[c]	$A_{960}/_{800}$[d]	$A_{1632}/_{1447}$[d]
Al-M(10)	10	4.48	1161	1.69	2.06	0.626
Al-M(20)	20	4.45	1242	1.65	2.04	0.592
Al-M(30)	30	4.47	1089	0.91	1.73	0.508
Al-M(40)	40	4.47	1133	0.62	1.57	0.418
Al-M(60)	60	4.45	1277	0.42	1.41	0.366
Al-M(80)	80	4.43	1148	0.23	1.03	0.318
Al-M(100)	100	4.43	1203	0.09	0.41	0.301

[a] Si/Al initial molar ratio in the synthesis gel.
[b] $a_0 = (2/\sqrt{3})d_{100}$.
[c] By ICP-OES.
[d] Integrated absorbance ratio of IR bands.

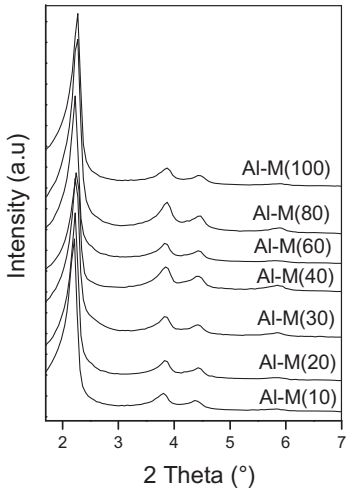

Fig. 1. XRD patterns of calcined samples synthesized with different Si/Al molar ratios.

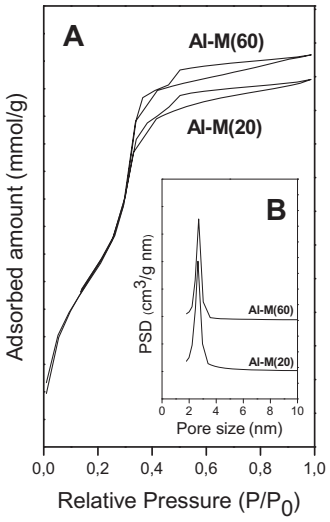

Fig. 2. (A) Nitrogen adsorption–desorption isotherms of calcined samples and (B) pore size distribution (PSD).

2θ range of 1–7° are indexed to the (100), (110) and (200) reflections, characteristic for hexagonal mesostructures. The results indicate that the well-ordered pore structure of MCM-41 was retained even for the sample with the higher Al content.

Table 1 shows the lattice parameter (a_0) for the synthesized samples (value about 4.45). The N_2 physisorption was carried out in order to complete the information about the structure of the samples. The adsorption–desorption isotherms of the Al-M(20) and Al-M(60) samples, taken as representative (Fig. 2) could be classified as type IV according to the IUPAC recommendation, typical of mesoporous structures. For a relative pressure (P/P_0) of around 0.1–0.25 these isotherms exhibit an inflection characteristic of capillary condensation within the uniform mesopores of the MCM-41 structure, which are called primary mesopores. The average pore diameter (Dp), calculated by the BJH method, was around of 2.74 nm for all the samples and therefore the wall thickness (W_t), calculated as a_0−Dp, was around 1.71 nm. In addition, the samples showed high specific surface (~1000 m^2g^{-1}) and pore volume (Vp ~ 0.83 cm^3/g), typical of mesoporous materials. These high values are consistent with the good structural order observed by XRD.

Measurements of transmission electron microscopy of the materials were made in order to examine their structural regularity. TEM images of representative Al-MCM-41 samples are shown in Fig. 3. The materials presented a well-defined mesoporous structure, exhibiting well-ordered parallel straight mesochannels characteristic of the hexagonal pore arrangement of MCM-41 type materials [44,45], which was also observed by us in the XRD patterns. The average mesopore sizes measured by TEM were in the 2.8–3.3 nm range. It should be noted that in Fig. 3(B) the image is viewed perpendicularly to the direction of the pore arrangement [46], clearly showing the presence of straight mesochannels arraying along the long axis [47]; meanwhile, the hexagonal arrangement of the unidirectional mesopores is clear in Fig. 3(A), (C) and (D) where a frontal view of them can be seen.

The SEM images of some samples taken as representative are shown in Fig. 4 (A–C). These images indicate the presence of particles that do not display any particular crystalline habit or morphology, although the spherical-like morphology seems to be the dominant one. The primary particles are very small and appear to be aggregated into larger secondary particles which exist in various sizes (5–8 μm). These apparently single particles observed in the SEM could be the result of intergrowth of multiple smaller particles [48].

3.2. Spectroscopic characterization

The Al content (wt.%) was determined by ICP-OES and is shown in Table 1. Moreover, it is important to highlight here the very low content of residual sodium in all of the samples (lower 0.2 wt.% for the Si/Al ratio = 20 and lower 0.07 wt.% for Si/Al ratio = 60).

As it has been shown by us [13], on the basis of a comparative FT-IR and NMR study, the infrared spectroscopy is able to provide evidence about the aluminum incorporation into the mesoporous framework. The infrared spectra in the 400–1600 cm^{-1} range for all the samples are shown in Fig. 5(A). The main bands described

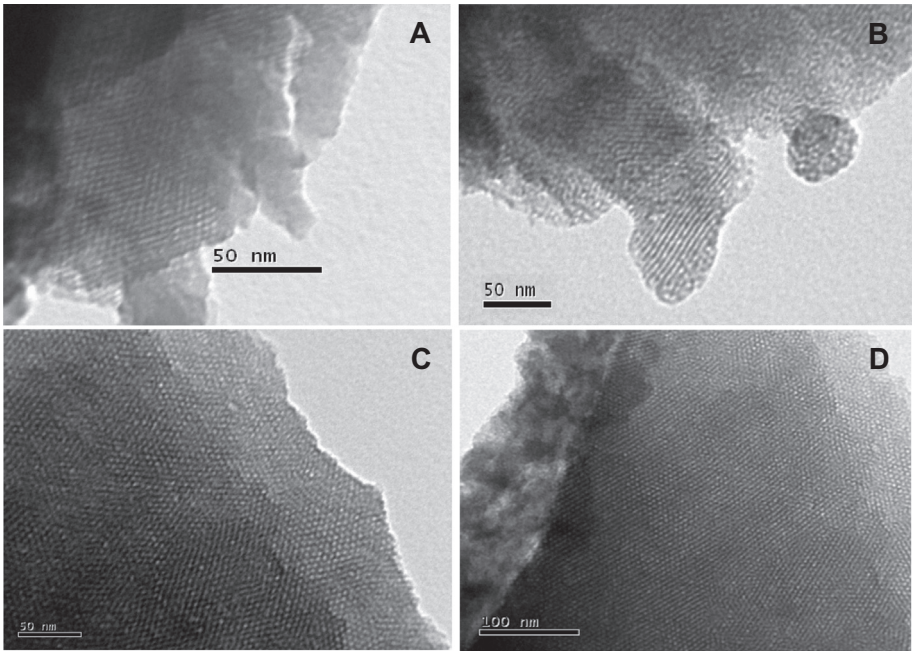

Fig. 3. Transmission electron microscopy images: (A) Al-M(10), (B–C) Al-M(20), (D) Al-M(100).

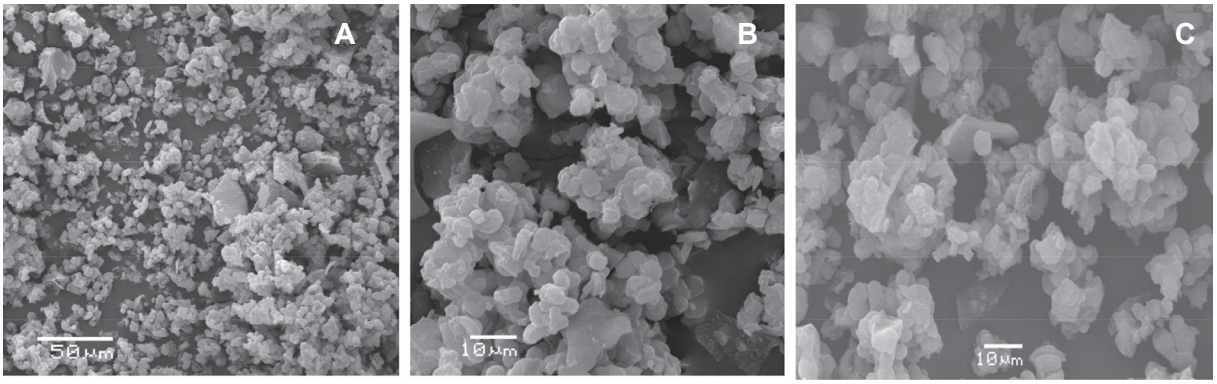

Fig. 4. Scanning electron micrographs of: (A) Al-M(10), (B) Al-M(20), (C) Al-M(100).

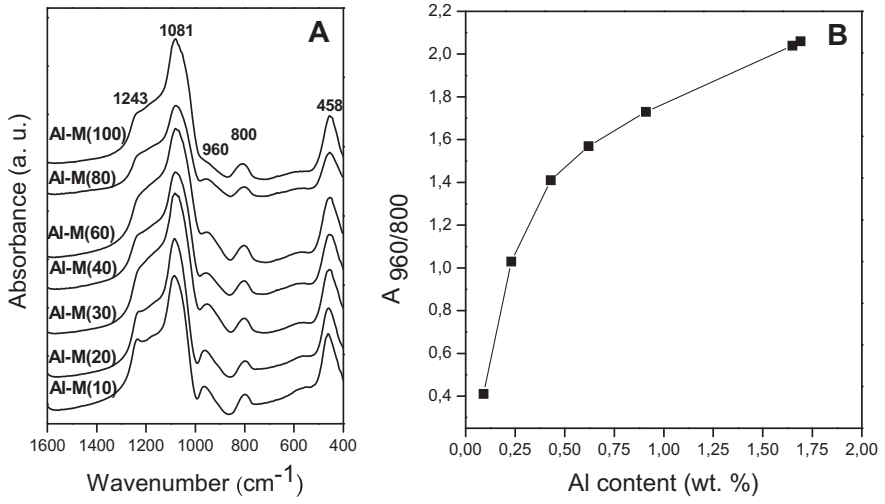

Fig. 5. (A) FT-IR spectra in the 400–1600 cm^{-1} range of the calcined samples synthesized with different Si/Al molar ratios. (B) $A_{960/800}$ integrated absorbances ratio vs. Al content in the final solids.

in the literature for MCM-41 are found in our samples [6,7,49,50]. Moreover, a band at 960 cm^{-1} [26,27,51,52], interpreted in terms of the overlapping of both Si–OH groups and Si–O–Al bonds vibrations, is clearly visible. Anyway, as it has been reported [13], the increase in the integrated absorbance of this band when the Al content increases can be considered a proof of the heteroatom incorporation replacing to Si into the framework [13]. Thus, we could observe in Fig. 5(B) how the integrated absorbance at 960 cm^{-1} with respect to the integrated absorbance at 800 cm^{-1} ($A_{960/800}$) increases with the Al amount increasing in the samples, which corroborates the above mentioned. Nevertheless, it should be note that this incorporation of Al, in tetrahedral coordination replacing to Si into the framework, is strongly increased for the lower Al contents, while the same is more slowly increased for the higher Al contents, probably due to the appearance of other Al species. These $A_{960/800}$ values are also summarized in the Table 1.

In order to detect the presence of silanol groups on the surface, Fig. 6 depicts the FT-IR spectra of the samples more representative in the hydroxyl range. It is known that there can be several types of surface silanol groups with different acidic properties: terminal, geminal, vicinal and nests [12,42,53–55]. All our spectra exhibited a broad and intense band, attributed to hydrogen bonded to hydroxyl groups [42,54], that could be deconvoluted into two contributions at about 3700 and 3590 cm^{-1}. According to the literature [12,42,53] these two contributions have been assigned to hydrogen bonded to vicinal silanol groups and silanol nests, respectively, generated at framework defect sites, probably due to the method used for catalyst preparation. Comparing the integrated absorbances of both contributions for the different samples, it is possible to observe that the relative proportion of silanol nests increases for the samples with higher Al contents which, at the same time, exhibit the higher framework aluminum amount (see Table 1 and Fig. 5). This fact would indicate that increasing the aluminum amount inside the framework, the formation of structural defects [54] is increased leading to a higher proportion of silanol nests.

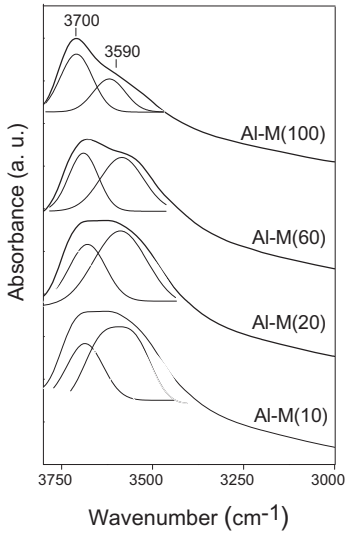

Fig. 6. FT-IR spectra in the hydroxyl stretching region of the calcined samples synthesized with different Si/Al molar ratios.

The chemisorption of pyridine followed by IR studies is usually a useful probe to detect the presence and nature of acid sites on a catalyst [56–59]. Fig. 7(A) shows the FT-IR spectra of adsorbed pyridine at room temperature on the samples synthesized with different Si/Al initial molar ratios. All our samples show bands at 1597 and 1447 cm^{-1} assigned to pyridine bonded to silanol groups whose hydroxyls are not capable to protonate pyridine [25,54,56–62]. However, evidence of some contribution to these bands from pyridine bonded to Lewis acid sites, probably arising from the presence of extra-framework aluminum oxide, has already been reported by us [6,7,13,63,64]. Such species would be very finely dispersed on the surface since they could not be detected either by XRD or TEM. On the other hand, the presence of a band at 1632 cm^{-1}, whose integrated absorbance is increased with the Al content increasing, has been attributed by us to pyridine interacting with acid hydroxyls [55,64,65], such as the nest silanols associated with the 3590 cm^{-1} band. Even if we have found that these acid sites are of a very weak character [13] Sato and co-workers [12] have reported that the nest silanol's acidity is the strongest of all the different silanol species [12,53]. Moreover, it is notable in these materials the lack of bridging Si(OH)Al hydroxyl groups strongly acid, frequently associated to a band at 1545 cm^{-1}. Taking into account that all of the measurements were affected by the wafer weight, the ratio between the integrated absorbances A_{1632} and A_{1447} ($A_{1632/1447}$) can be semi-quantitatively employed to estimate the relative density of the acid hydroxyl

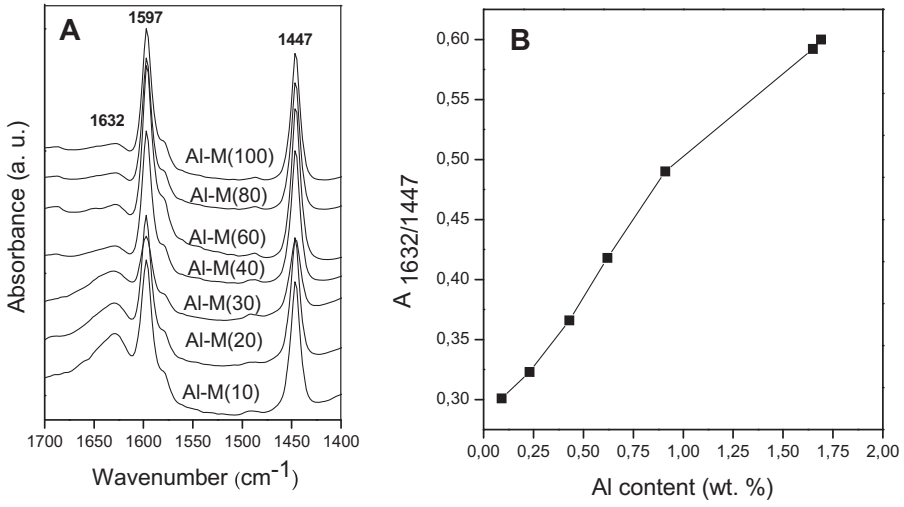

Fig. 7. (A) FT-IR of pyridine adsorbed at room temperature on calcined samples synthesized with different Si/Al molar ratios. (B) $A_{1632/1447}$ integrated absorbances ratio vs. Al content in the final solids.

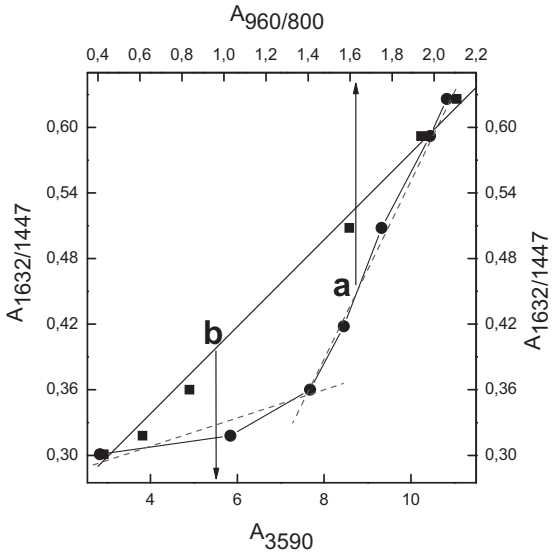

Fig. 8. $A_{1632/1447}$ vs. (a) $A_{960/800}$ and (b) A_{3590}.

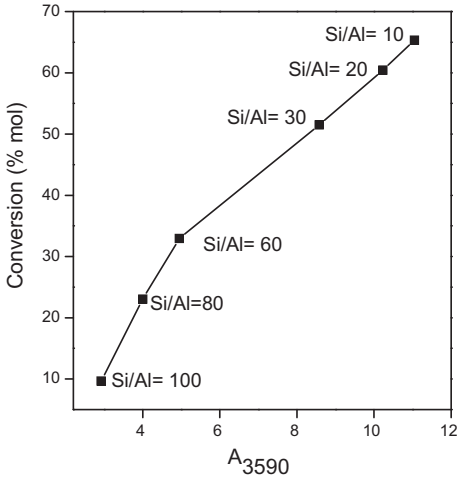

Fig. 9. CHO conversion vs. A_{3590} integrated absorbance.

sites. These $A_{1632/1447}$ values are also summarized in Table 1. In order to shed light on the origin of this acidity in these materials, this parameter ($A_{1632/1447}$) has been graphed vs. the Al content in Fig. 7(B), as well as vs. the $A_{960/800}$ integrated absorbances ratio (as indicative of the Al incorporation into framework) and the integrated absorbance of the 3590 cm^{-1} IR band (A_{3590}) (associated to nest silanols) (Fig. 8). As it can be seen in Fig. 7B the slope of the curve is diminished for Al contents above 1 wt.%, probably due to the presence of other acid species such as the aluminum oxide which mainly presents Lewis acidity. On the other hand, it is observed in Fig. 8 (curve a) that while initially the acidity associated to the acid hydroxyls ($A_{1632/1447}$) is slowly increased with the framework Al increasing, the same is very strongly increased for the samples with higher Al incorporation inside the structure (above $A_{960/800}$ = 1.4). Likewise, it is very clear the linear increase in the acid hydroxyls density when the concentration of nest silanols (A_{3590}) increases (curve b in Fig. 8). Therefore, these observations confirm that the acidity of our samples arising from hydroxyl groups (silanols) is due to the silanol nests. These species would be mainly generated from the introduction of Al inside the framework and their acid properties would be caused by an inductive effect of the heteroatom present. Thus, changes in the electron density around Si due to charge unbalance, or differences in electronegativity or local structure deformation resulting from the Al incorporation may weaken the Si-O-H bond in the silanol nests giving them the acid properties. Then above a critical proportion of framework Al ($A_{960/800}$ = 1.4, corresponding to a Si/Al ratio = 60), the formation of these structural defects would be quickly increased, leading to a density of nest silanols (responsible of the observed acidity) strongly increasing with the framework Al amount. This feature is giving account for the higher slope of the curve (a) in Fig. 8 for $A_{960/800}$ ratios above 1.4.

3.3. Catalytic Activity

In a previous work [13] we have evaluated catalytically this materials type in the vapor-phase Beckmann rearrangement of the CHO, finding a relationship between the yield to ε-caprolactam and the acid silanols density on the catalysts. We proposed that these weakly acid hydroxyl groups present in silanols nests, arising from the introduction of Al inside the framework, are actually the active sites for achieve the Beckmann rearrangement of the CHO with a very high selectivity toward ε-caprolactam.

In this work, we show the catalytic results for this reaction over Al-MCM-41 catalysts synthesized with different Al contents in the synthesis gel, which are able to introduce different concentrations of nest silanols into the structure. Thus the CHO conversion vs. the integrated absorbance of the 3590 cm^{-1} IR band (A_{3590}) (associated to nest silanols) is shown in Fig. 9. As it is observed, the conversion values are increased according with the nest silanols density increasing. Nevertheless, a strictly linear behavior was not observed, probably due to a minor accessibility of the active sites to the reactive when the Al loading is increasing. Then, varying the Al content in the synthesis gel we have achieved to increase the weakly acid silanol nests density on the material and to reach a conversion about 66% for a Si/Al initial ratio of 10. In addition, the ε-caprolactam selectivity was maintained in 100% for all the Al contents, indicating that the acid strength of the nest silanols generated by increasing the Al content was kept sufficiently weak to not catalyze the formation of by-products. In this sense, it should to be noted that the coke formation was insignificant [13]. Therefore, the presence of species adsorbed on catalyst surface, which could poison the active sites, could be discarded under the mild reaction conditions employed in these experiments.

Finally, at this moment, the reaction parameters (temperature, *W*/*F* and solvent) are being modified to study their effect on the activity and selectivity in order to reaching higher conversion values and maximize the ε-caprolactam yield.

4. Conclusion

Aluminum modified mesoporous molecular sieves with MCM-41 structure were prepared by the direct hydrothermal synthesis method. The effect of different Al contents in the catalysts on their structural, acid and catalytic properties was investigated. The hexagonal pore arrangement typical of MCM-41 materials was clearly visualized by TEM and inferred by XRD. The employed synthesis procedure leads to the incorporation of Al in tetrahedral coordination into the framework and the formation of silanol nests at framework defect sites, which increase with the Al content increasing. We have found that the weakly acid character from hydroxyl groups present in our samples is purely caused by these nest silanols. Moreover, a critical proportion of framework Al ($A_{960/800}$ ratio = 1.4 corresponding to a Si/Al molar ratio = 60) seems to be

necessary to generate such nests, after which the density of acid nest silanols is strongly increased with the framework Al amount increasing. In addition, evidence of Lewis acidity could be related to the presence of aluminum oxide species, which would be very finely dispersed on the surface since they could not be detected either by XRD or TEM. The catalytic activity of these materials was evaluated for the reaction of Beckmann rearrangement of CHO. By varying the Al content in the synthesis gel, we have achieved to increase the density of acid nest silanols, responsible of the activity, up to reach a CHO conversion about 66% (for a Si/Al molar ratio = 10). The ε-caprolactam selectivity was maintained in 100% for all of the Al contents, indicating that the acid strength of the active sites was kept sufficiently weak to not catalyze the formation of by-products.

References

[1] C.T. Kresge, M.E. Leonowicz, W.J. Roth, J.C. Vartuli, J.S. Beck, Nature 359 (1992) 710–712.
[2] J.S. Beck, J.C. Vartuli, W.J. Roth, M.E. Leonowicz, C.T. Kresge, K.D. Schmitt, C.T.-W. Chu, D.H. Olson, E.W. Sheppard, S.B. McCullen, J.B. Higgins, J.L. Schlenker, J. Am. Chem. Soc. 114 (1992) 10834–10843.
[3] W. Kolodziejski, A. Corma, M.T. Navarro, J. Perez Pariente, Solid State Nucl. Magn. Reson. 2 (1993) 253–259.
[4] P.T. Tanev, M. Chibwe, T.J. Pinnavaia, Nature 368 (1994) 321–323.
[5] R. Schmidt, D. Akporiaye, M. Stöcker, O.H. Ellestad, J. Chem. Soc. Chem. Commun. (1994) 1493–1495.
[6] G.A. Eimer, L.B. Pierella, G.A. Monti, O.A. Anunziata, Catal. Lett. 78 (2002) 65–75.
[7] G.A. Eimer, L.B. Pierella, G.A. Monti, O.A. Anunziata, Catal. Commun. 4 (2003) 118–123.
[8] K. Kalyanasundaraman, J.K. Thomas, J. Phys. Chem. 80 (1976) 1462–1473.
[9] C.M. Chanquía, A.L. Cánepa, K. Sapag, P. Reyes, E.R. Herrero, S.G. Casuscelli, G.A. Eimer, Top. Catal. 54 (2011) 160–169.
[10] M. Busio, J. Jänchen, J.H.C. Van Hooff, Micropor. Mater. 5 (1995) 211–218.
[11] A. Corma, V. Fornes, M.T. Navarro, J. Perez-Pariente, J. Catal. 148 (1994) 569–574.
[12] Y. Izumi, H. Ichihashi, Y. Shimazu, M. Kitamura, H. Sato, Bull. Chem. Soc. Jpn. 80 (7) (2007) 1280–1287.
[13] E.G. Vaschetto, G.A. Monti, E.R. Herrero, S.G. Casuscelli, G.A. Eimer, Appl. Catal. A 453 (2013) 391–402.
[14] Kirk-Othmer, Encyclopedia of Chemical Technology, fourth ed., vol. 4, Wiley, New York, 1995. pp. 827–839.
[15] P.B. Venuto, P.S. Landis, Adv. Catal. 18 (1968) 259–371.
[16] A. Aucejo, M.C. Burguet, A. Corma, V. Fornes, Appl. Catal. 22 (1986) 187–200.
[17] W.K. Bell, C.D. Chang, European Patent 056 (1985) 698.
[18] H. Sato, N. Ishii, K. Hirose, S. Nakamura, Stud. Surf. Sci. Catal. 28 (1986) 755–762.
[19] K. Chaudhari, R. Bal, A.J. Chandwadkar, S. Sivasanker, J. Mol. Catal. A 177 (2002) 247–253.
[20] L. Forni, C. Tosi, G. Fornasari, F. Trifiró, A. Vaccari, J.B. Nagy, J. Mol. Catal. A 221 (2004) 97–103.
[21] A.-N. Ko, C.-C. Hung, C.-W. Chen, K.-H. Ouyang, Catal. Lett. 71 (2001) 219–224.
[22] D. Zhang, R. Wang, X. Yang, Catal. Commun. 12 (2011) 399–402.
[23] C. Ngamcharussrivichai, P. Wu, T. Tatsumi, Catal. Commun. 8 (2007) 135–138.
[24] T.D. Conesa, J.M. Campelo, D. Luna, J.M. Marinas, A.A. Romero, Appl. Catal. B 70 (2007) 567–576.
[25] T.D. Conesa, J.M. Hidalgo, R. Luque, J.M. Campelo, A.A. Romero, Appl. Catal. A 299 (2006) 224–234.
[26] D. Mao, G. Lu, Q. Chen, Appl. Catal. A 279 (2005) 145–153.
[27] B.-Q. Xu, S.-B. Cheng, X. Zhang, S.-F. Ying, Q.-M. Zhu, Chem. Commun. (2000) 1121–1122.
[28] L. Forni, G. Fornasari, C. Tosi, F. Trifiro, A. Vaccari, F. Dumeignil, J. Grimblot, Appl. Catal. A 248 (2003) 47–57.
[29] T. Curtin, J.B. McMonagle, B.K. Hodnett, Catal. Lett. 17 (1993) 145–150.
[30] H. Ichihashi, M. Kitamura, Catal. Today 73 (2002) 23–28.
[31] H. Kath, R. Glaser, J. Weitkamp, Chem. Eng. Technol. 24 (2001) 150–153.
[32] C. Flego, L. Dalloro, Micropor. Mesopor. Mater. 60 (2003) 263–271.
[33] T. Takahashi, T. Kai, E. Nakao, Appl. Catal. A 262 (2004) 137–142.
[34] G.P. Heitmann, G. Dahlhoff, J.P.M. Niederer, W.F. Hölderich, J. Catal. 194 (2000) 122–129.
[35] C.-C. Tsai, C.-Y. Zhong, I. Wang, S.-B. Liu, W.-H. Chen, T.-C. Tsai, Appl. Catal. A 267 (2004) 87–94.
[36] G. Dahlhoff, U. Barsnick, W.H. Hölderich, Appl. Catal. A 210 (2001) 83–95.
[37] E.R. Herrero, O.A. Anunziata, L.B. Pierella, O.A. Orio, Latin Am. Appl. Res. 24 (1994) 195–202.
[38] G.P. Heitmann, G. Dahlhoff, W.F. Hölderich, Appl. Catal. A 185 (1999) 99–108.
[39] L.-X. Dai, R. Hayasaka, Y. Iwaki, K.A. Koyano, T. Tatsumi, Chem. Commun. (1996) 1071–1072.
[40] T. Yashima, K. Miura, T. Komatsu, Stud. Surf. Sci. Catal. 84 (1994) 1897–1904.
[41] P. O'Sullivan, L. Forni, B.K. Hadnett, Ind. Eng. Chem. Res. 40 (2001) 1471–1475.
[42] W.F. Hölderich, J. Roseler, G. Heitmann, A.T. Liebens, Catal. Today 37 (1997) 353–366.
[43] T. Ushikubo, K. Wada, J. Catal. 148 (1994) 138–148.
[44] S. Rodrigues, S. Uma, I. Martyanov, K.J. Klabunde, J. Photochem. Photobiol. A 1–3 (165) (2004) 51–58.
[45] V.R. Elías, E.V. Sabre, K. Sapag, S.G. Casuscelli, G.A. Eimer, Appl. Catal. A 413–414 (2012) 280–291.
[46] K. Choi, R. Wakabayashi, T. Tatsumi, T. Yokoi, K. Kuroda, J. Colloid Interface Sci. 359 (2011) 240–247.
[47] Y. Xu, G. Zhou, C. Wu, T. Li, H. Song, Solid State Sci. 13 (2011) 867–874.
[48] M.A. Betiha, S.A. Mahmoud, M.F. Menoufy, A.M. Al-Sabagh, Appl. Catal. B 3–4 (107) (2011) 316–326.
[49] G.A. Eimer, S.G. Casuscelli, G.E. Ghione, M.E. Crivello, E.R. Herrero, Appl. Catal. A 298 (2006) 232–242.
[50] A. Palani, N. Gokulakrishnan, M. Palanichamy, A. Pandurangan, Appl. Catal. A 304 (2006) 152–158.
[51] L. Cedeño, D. Hernandez, T. Klimova, J. Ramirez, Appl. Catal. A 241 (2003) 39–50.
[52] A. Corma, Chem. Rev. 97 (1997) 2373–2419.
[53] H. Ichihashi, Sci. Technol. 145 (2002) 73–84.
[54] A. Jentys, K. Kleestorfer, H. Vinek, Micropor. Mesopor. Mater. 27 (1999) 321–328.
[55] V.L. Zholobenko, D. Plant, A.J. Evans, S. Holmes, Micropor. Mesopor. Mater. 44 (2001) 793–799.
[56] C.M. Chanquía, L. Andrini, J.D. Fernández, M.E. Crivello, F.G. Requejo, E.R. Herrero, G.A. Eimer, J. Phys. Chem. C 114 (2010) 12221–12229.
[57] B. Chakraborty, B. Viswanathan, Catal. Today 49 (1999) 253–260.
[58] M. Hunger, U. Schenk, M. Breuninger, R. Gläser, J. Weitkamp, Micropor. Mesopor. Mater. 27 (1999) 261–271.
[59] X.S. Zhao, G.Q. Lu, A.K. Whittaker, G.J. Millar, H.Y. Zhu, J. Phys. Chem. B 101 (1997) 6525–6531.
[60] G.A. Eimer, S.G. Casuscelli, C.M. Chanquia, V.R. Elías, M.E. Crivello, E.R. Herrero, Catal. Today 133 (2008) 639–646.
[61] D. Trong On, S.V. Nguyen, V. Hulea, E. Dumitriu, S. Kaliaguine, Micropor. Mesopor. Mater. 57 (2003) 169–180.
[62] D. Srinivas, R. Srivastava, P. Ratnasamy, Catal. Today 96 (2004) 127–133.
[63] R. Mokaya, W. Jones, Z. Luan, M.D. Alba, J. Klinowski, Catal. Lett. 37 (1996) 113–120.
[64] C. Otero Arean, M. Rodriguez Delgado, V. Montouillout, J.C. Lavalley, C. Fernandez, J.J. Cuart Pascual, J.B. Parra, Micropor. Mesopor. Mater. 67 (2004) 259–264.
[65] E. Escalona Platero, M. Peñarroya Mentruit, C. Otero Areán, A. Zecchina, J. Catal. 162 (1996) 268–276.